

Clustering-based Joint Channel Estimation and Signal Detection for NOMA

Ayoob Salari, *Student Member, IEEE*, Mahyar Shirvanimoghaddam, *Senior Member, IEEE*, Muhammad Basit Shahab, *Member, IEEE*, Reza Arablouei, Sarah Johnson, *Member, IEEE*

Abstract

We propose a joint channel estimation and signal detection approach for the uplink non-orthogonal multiple access using unsupervised machine learning. We apply the Gaussian mixture model to cluster the received signals, and accordingly optimize the decision regions to enhance the symbol error rate (SER). We show that, when the received powers of the users are sufficiently different, the proposed clustering-based approach achieves an SER performance on a par with that of the conventional maximum-likelihood detector with full channel state information. However, unlike the proposed approach, the maximum-likelihood detector requires the transmission of a large number of pilot symbols to accurately estimate the channel. The accuracy of the utilized clustering algorithm depends on the number of the data points available at the receiver. Therefore, there exists a tradeoff between accuracy and block length. We provide a comprehensive performance analysis of the proposed approach as well as deriving a theoretical bound on its SER performance as a function of the block length. Our simulation results corroborate the effectiveness of the proposed approach and verify that the calculated theoretical bound can predict the SER performance of the proposed approach well.

Index Terms

Cluster analysis, Gaussian mixture model, joint detection and estimation, massive IoT, non-orthogonal multiple access, unsupervised machine-learning.

Ayoob Salari and Mahyar Shirvanimoghaddam are with the School of Electrical and Information Engineering, The University of Sydney, Camperdown, NSW 2006, Australia (e-mail: ayoob.salari@sydney.edu.au; mahyar.shirvanimoghaddam@sydney.edu.au)

Muhammad Basit Shahab and Sarah Johnson are with the School of Engineering, University of Newcastle, Callaghan, NSW 2308, Australia (e-mail: basit.shahab@newcastle.edu.au; sarah.johnson@newcastle.edu.au).

Reza Arablouei is with the Commonwealth Scientific and Industrial Research Organisation, Pullenvale, QLD 4069, Australia (e-mail: reza.arablouei@csiro.au).

I. INTRODUCTION

The fifth generation (5G) of mobile standards has introduced two main service categories, namely, massive machine-type communications (mMTC) and ultra-reliable low-latency communications (URLLC) [1], besides the enhanced mobile broadband (eMBB) that has been the primary focus of all previous generations. While the main focus of URLLC is to provide high reliability and low latency, mMTC mainly emphasizes handling a huge number of low-throughput, delay-tolerant, energy-efficient, and low-cost devices, which are usually used in Internet of things (IoT) applications. A recent forecast estimates the enterprise and automotive IoT devices to grow from 5.8 billion in 2020 to 41.6 billion in 2025, generating 79.4 zettabytes of data [2]. While 5G is expected to serve many IoT applications, major breakthroughs in designing communication protocols and radio resource management techniques are required to serve applications with a diverse range of requirements in terms of data rate, reliability, availability, end-to-end latency, energy efficiency, security, and privacy.

The non-orthogonal multiple access (NOMA) schemes have gained significant attention in the last decade as an enabler for mMTC [3]–[5]. NOMA allows multiple users to share the same radio resources leading to higher spectral efficiency. Two main categories of NOMA are power-domain and code-domain [6]. While, in power-domain NOMA, users transmit with different power levels depending on their channel conditions, code-domain NOMA relies on assigning unique codes to the users. Some prominent code domain NOMA techniques are sparse code multiple access (SCMA) [7], multi-user shared access (MUSA) [8], interleave-division multiple access (IDMA) [9], and low-density spreading (LDS) [10]. There are also other NOMA techniques such as bit division multiplexing (BDM) [11] and pattern division multiple access (PDMA) [12]. Power-domain NOMA is compatible with the current communication networks and can improve spectral efficiency over the same bandwidth. Code-domain NOMA requires higher bandwidth and significant changes in the current systems [13].

Not only does NOMA allow multiple devices to share the same radio resources boosting the network capacity significantly, but it can also reduce the signaling overhead and latency by allowing the grant-free uplink connection [14]. Current wireless networks allocate data transmission slots to users through a process called random access that is a multi-step handshake between the base station (BS) and the user. When there are many of users, which is the case in massive IoT, this grant-based access suffers from excessive signaling overhead that take up significant resources to establish a connection. This problem is even more challenging in the grant-free access since we also need to consider access collisions and we do not have sufficient knowledge regarding the participant users. Subsequently, it can result in a substantial efficiency loss since the typical data size is comparable to the overhead signal. Incorporation of NOMA

with grant-free access that is a lightweight random access protocol is considered to be a key enabler of massive connectivity in IoT [15].

With the massive IoT in 5G and beyond, the network will be highly complex due to scale, density, and heterogeneity. It will also be highly dynamic with numerous possibly contending design requirements. Moreover, for efficient communications, there are many optimization parameters because of channel and hardware impairments [16], [17]. Machine learning (ML) can be effectively used to enhance network intelligence and enable self-adaptability. By analyzing the patterns in the data and learning through them, ML algorithms are capable of handling highly complex dynamic networks in an efficient and timely manner [18]. ML is capable of rendering effective and efficient services in different layers of networks. In the physical layer, clustering methods, such as k-means and Gaussian mixture model (GMM) can be performed for channel estimation and signal detection, convolutional neural network (CNN) algorithms can be applied for channel decoding, and complex CNNs can be adopted to build OFDM [19]. In the data link layer, supervised learning and deep neural network (DNN) algorithms can be utilized for user scheduling and operation of automatic repeat request (ARQ) or hybrid ARQ to enhance the reliability. Moreover, in the network layer, reinforcement learning can be applied to improve the network robustness and guarantee service continuity [20], [21].

Channel estimation schemes can be mainly categorized into training-based [22], blind [23], and semi-blind [24] schemes. Training-based schemes use long training sequences to obtain the channel state information (CSI) with low complexity but decrease throughput [22]. In contrast, by using the properties of the transmitted signal, blind channel estimation schemes estimate the channel with no training symbol [23]. While these schemes are bandwidth efficient, they are more complex and less accurate in comparison with training-based schemes. To strike a balance between throughput, accuracy, and complexity, semi-blind schemes combine the merits of both training-based and blind schemes [25]. Recently, there has been a growing interest in joint channel estimation and signal detection for grant-free NOMA [26]–[28]. By representing the joint problem as a compressed sensing problem, the authors of [29]–[31] utilized the sparsity of the pilot (training) symbols to reduce the number of training symbols [26]. However, in massive IoT, since the packets are small, even a few training symbols can lead to a major efficiency loss. One intuitive way to reduce the number of training symbols with no significant loss of performance is to apply ML algorithms, particularly unsupervised clustering techniques [32].

In this paper, we propose a new approach for joint channel estimation and user detection in uplink NOMA using minimal training symbols and no explicit estimation of the CSI at the receiver. We employ an unsupervised ML algorithm, that is based on a Gaussian mixture model (GMM), to cluster the received signals at the receiver side. Given a model for the joint statistical distribution of some observed variables,

the maximum likelihood estimation (MLE) can be used to estimate the parameters of the model. While MLE is asymptotically efficient, it may be biased, especially with a small sample size [33]. When there exists missing data or the model depends on unobserved latent variables, canonical MLE is not applicable [34]. In such cases, the expectation-maximization (EM) algorithm is useful for estimating the model parameters [35], [36]. The EM algorithm is a two-step iterative method. In the expectation step (E-step), given the observed data, the expected value of the complete-data log-likelihood is estimated. In the maximization step (M-step), the expected value in the previous step is maximized to update the parameter estimates [37]. EM is numerically stable and each iteration increases the likelihood [38].

GMM is used to approximate the probability distribution function of the observations via the mixture of a set of Gaussian probability distribution functions. The mixture parameters can be estimated using an appropriate algorithm that is often based on MLE or EM. When the number of the mixture components is not known, the problem is further compounded as a model selection problem. The number of components can be estimated using certain statistical approaches [39]. The global convergence of the EM algorithm fitting a GMM model with two Gaussian distributions with similar densities is guaranteed, as long as it is initialized in the neighborhood of the desired solution [40]. For higher-order mixture models, if the GMM centers (the means of the Gaussian components) are well separated, EM converges locally to the global optimum [41], [42] with a convergence rate higher than that of the quasi-Newton algorithm [43]. The lower and upper bounds for the number of samples required to estimate the parameters of a GMM of well-separated centers with any given accuracy is calculated in [44], [45]. Authors of [45] show that for a GMM with M components, EM converges under the cluster separation of $\Omega(\sqrt{\log M})$ rather than $\Omega(\sqrt{M})$, which was previously presumed [41], [42].

In this paper, we propose a new algorithm for joint user detection and channel estimation using GMM-based clustering. We use data clustering results to estimate the channels and perform successive interference cancellation (SIC) to detect each user's signal. We show that when the powers of the signals received from the users are sufficiently different, the proposed clustering-based approach with no CSI at the receiver achieves the same performance in terms of symbol error rate (SER) as the conventional MLE-based detector with full CSI. We also show that the performance of the proposed approach is governed by a tradeoff between accuracy and block length as the accuracy of clustering depends on the number of data points (symbols) available at the receiver. This paper is an extension to our work previously published as [32]. Our main contributions in this paper are listed below.

- We propose a novel joint channel estimation and signal detection algorithm using GMM-based clustering that not only reduces the number of pilot symbols but also improves the error rate. This technique can be of great benefit for massive IoT systems, where the packets are short and even a

few pilot symbols have substantial effect on the throughput of the system.

- We develop an analytical framework to characterize the theoretical bounds on the SER performance of the proposed technique. In particular, we consider the difference between the exact value of parameters and the estimated values using the EM method. We present a theorem to find an upper-bound on this error and use that to calculate SER.
- We present extensive numerical results to compare our proposed model with the current practical semi-blind estimation techniques and optimal MLE method with full CSI with multiple users.

The rest of the paper is organized as follows. We present the system model and provide some relevant preliminary information in Section II. We describe our proposed GMM-clustering-based approach for joint channel estimation and signal detection in Section III. Section IV characterizes the theoretical bounds on the SER. We provide extensive numerical results for evaluating the performance of the proposed approach in Section IV. We provide some discussions in Section V and conclude the paper in Section V.

Notations: Matrices, vectors, and scalars are denoted by uppercase boldface, lowercase boldface, and lowercase italic letters, e.g., \mathbf{A} , \mathbf{a} , and a , respectively. The transpose, Hermitian, and inverse of \mathbf{A} are denoted by \mathbf{A}^T , \mathbf{A}^H , and \mathbf{A}^{-1} , respectively. The $N \times N$ identity matrix and the $N \times N$ matrix consisting of all zero entries are denoted by \mathbf{I}_N and $\mathbf{0}_N$, respectively. Notations $\|\mathbf{a}\|$ and $\|\mathbf{A}\|_F$ denote the ℓ_2 -norm of \mathbf{a} and the Frobenius norm of \mathbf{A} , respectively.

II. SYSTEM MODEL

We consider an uplink scenario, where a set of U users use NOMA to transmit their data to a base station (BS). The BS and users are assumed to be fixed and equipped with a single antenna. We denote the channel between the u -th user, $u \in \mathcal{U} = \{1, \dots, U\}$, and the BS by h_u . Furthermore, we assume a block fading channel model so that the channel remains constant over a block time and changes independently across blocks.

Unlike orthogonal multiple access (OMA) in which a radio resource is allocated to only a single user, in NOMA, the signals of multiple users may share a single radio resource. Therefore, the received signal at the BS at time instant i can be written as

$$y_i = \sum_{u=1}^K \sqrt{P_u} h_u x_{u,i} + n_i, \quad (1)$$

where K is the number of active users, P_u is the power of user u , $x_{u,i}$ is the transmitted symbol of user u at time instant i satisfying $\mathbb{E} [|x_{u,i}|^2] = 1$, and n_i is the circularly symmetric additive white Gaussian noise (AWGN) with zero mean and unit variance, i.e., $n_i \sim \mathcal{CN}(0, 1)$. We assume that h_u , n_i , and $x_{u,i}$

are statistically independent of each other. Furthermore, we define the SNR of user u , denoted by γ_u , as P_u divided by the power of noise.

The user symbols $x_{u,i}$ are modulated using a common modulation scheme with the signal constellation \mathcal{S} and cardinality $|\mathcal{S}|$, i.e., each $x_{u,i}$ is randomly and uniformly drawn from \mathcal{S} . For simplicity, we assume that all users use the quadrature phase shift keying (QPSK) modulation scheme when transmitting their signals, i.e., $x_{u,i} \in \{\exp(\frac{-j\pi}{4}), \exp(\frac{-j3\pi}{4}), \exp(\frac{j\pi}{4}), \exp(\frac{j3\pi}{4})\}$, $\forall u \in \{1, \dots, K\}$ and $i \in \{1, \dots, N\}$ ¹, where N is the number of symbols that each user transmits. It is easy to show that y_i are i.i.d. and have the following Gaussian mixture distribution

$$y_i \sim \frac{1}{|\mathcal{S}|^K} \sum_{\mathbf{x}_i \in \mathcal{S}^K} \mathcal{CN}(\mathbf{h}^T \mathbf{x}_i, 1) \quad (2)$$

where $\mathbf{h} \in \mathbb{C}^{K \times 1}$ stacks the channels h_u of all users and $\mathbf{x}_i \in \mathbb{C}^{K \times 1}$ their signals $x_{u,i}$.

Throughout the paper, we assume that all users are frame synchronized. This can be achieved by frequently sending beacon signals from the BS [46]. We also assume that the BS does not know the CSI to any user. Therefore, it attempts to jointly estimate the channels and detect the signals. However, we assume that the BS knows the number of transmitting users, K , and the utilized modulation scheme. Later in Section VI, we show how the assumption of knowing the number of users at the BS can be relaxed.

III. CLUSTERING-BASED JOINT CHANNEL ESTIMATION AND SIGNAL DETECTION

To better understand the proposed joint channel estimation and signal detection approach, we first discuss Fig. 1 that shows the collected signals at the receiver in the I-Q plane. Fig. 1a shows the received signals for a point-to-point (single user) communication system. Figs. 1b and 1c show the received signals for a two-user NOMA communication system, when both users use the QPSK modulation. As seen in Fig. 1a, for a single active user, the received signals at the BS can be grouped into four clusters and the centroid of each cluster can be used to estimate the amplitude and phase of the channel. When the number of active users is increased by one, the signals of both users can be grouped into 16 clusters as the BS knows the number of active users (Fig. 1b). When the clusters are distinct from each other, the phase and amplitude of the channels between the BS and the users can be estimated accurately. However, when channel fading and noise cause the clusters to overlap (Fig. 1c), estimation of the channels and detection of the signals is challenging. In what follows, we propose an effective method to cluster the received signals and estimate the channels and detect the user signals jointly.

¹The proposed approach can be easily extended to consider more complex constellations.

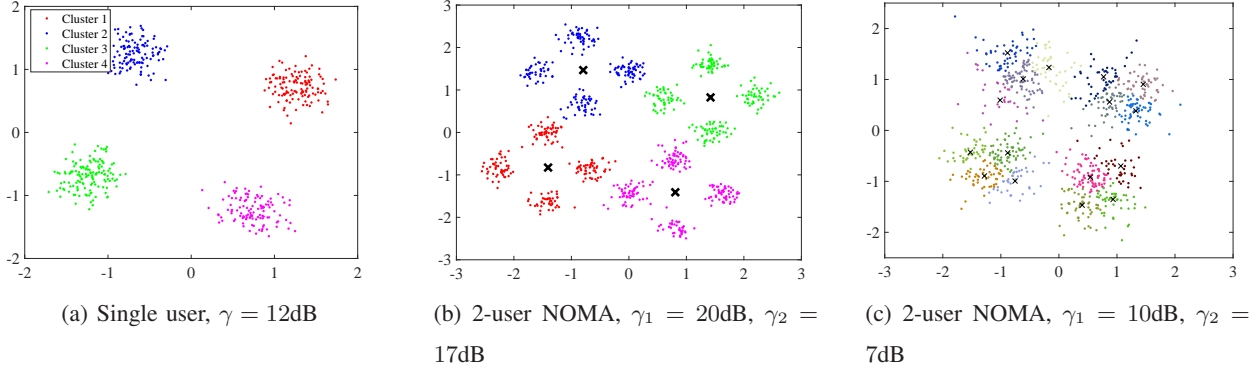


Fig. 1: Received signal constellation diagram at the BS for $N = 500$ and different values of SNR (γ_u).

There are several prominent clustering algorithms, such as k -means, DBSCAN [47], OPTICS [48], [49], mean shift [50], and GMM [51], that can be used to cluster the received signals. Since channels are block-fading and all users employ the same modulation scheme, the clusters at the BS are symmetric in the IQ plane with roughly the same densities (see Fig. 1). Owing to the fact that the noise has Gaussian distribution, the received signals at the BS can be modeled using a mixture of Gaussian distributions (2). Hence, GMM is a good choice for our clustering problem.

A. GMM-based Clustering

SIC recovers the multiplexed user signals from the received superimposed signals in the decreasing order of their received powers at the BS. Initially, the receiver decodes the signal of the strongest user (the user with the highest received power). It then reconstructs and removes it from the received signal. Afterwards, it decodes the next strongest signal and so on. In order to apply the SIC at the BS, we start by dividing the received signals (data points) into four clusters, which represent user 1's signals. Next, we select each of those four clusters and split them further into four clusters representing user 2's signals and so on. Taking the received signals as our observed data, the considered joint channel estimation and signal detection problem boils down to estimating the unknown latent parameters of the assumed Gaussian mixture distribution in (2).

Since we assume that the noise affecting the received signals is i.i.d. AWGN, from a theoretical point of view, one may conclude that the GMM clustering used in our proposed algorithm is equivalent to the well-known K -means clustering algorithm. However, in practice, the noise covariance matrix is not strictly a multiple of the identity matrix, i.e., the noise affecting different received signals may be correlated or have different variances. Therefore, the GMM clustering is more accurate compared with

the K -means clustering as, unlike K -means, it does not assume the same covariance for all clusters but estimates them for each cluster.

Since the received signals are represented as complex numbers, we denote a 2-dimensional multivariate Gaussian probability density function by $g(\mathbf{z}; \boldsymbol{\mu}, \boldsymbol{\Sigma})$ where $\boldsymbol{\mu}$ and $\boldsymbol{\Sigma}$ are the mean vector and the covariance matrix, respectively, and express it as

$$g(\mathbf{z}; \boldsymbol{\mu}, \boldsymbol{\Sigma}) = \frac{\exp\left(-\frac{1}{2}(\mathbf{z} - \boldsymbol{\mu})^T \boldsymbol{\Sigma}^{-1}(\mathbf{z} - \boldsymbol{\mu})\right)}{\sqrt{(2\pi)^2 |\boldsymbol{\Sigma}|}}. \quad (3)$$

In GMM clustering, the number of clusters is known and the data is assumed to be generated by a mixture of Gaussian distributions. A GMM parameterizes the mean, covariance, and weight of each Gaussian distribution component. When a common M -ary modulation scheme is adopted by all users, there are M Gaussian distributions each with weight ω_j , $j \in \{1, \dots, M\}$. Accordingly, the underlying Gaussian mixture distribution can be written as a weighted sum of the M constituent Gaussian distributions (each representing a cluster), i.e.,

$$p(\mathbf{z}; \boldsymbol{\mu}_1, \dots, \boldsymbol{\mu}_M, \boldsymbol{\Sigma}_1, \dots, \boldsymbol{\Sigma}_M) = \sum_{j=1}^M \omega_j g_j(\mathbf{z}; \boldsymbol{\mu}_j, \boldsymbol{\Sigma}_j) \quad (4)$$

where $\sum_{j=1}^M \omega_j = 1$. We are interested in estimating $\boldsymbol{\mu}_j$, $\boldsymbol{\Sigma}_j$, and ω_j , $j = 1, \dots, M$, from the observed data. This can be done by maximizing the likelihood function (4) for all received signals. To this end, we utilize the expectation-maximization (EM) algorithm [37] that is suitable for solving maximum likelihood problems with unobserved latent variables.

We define the corresponding log-likelihood function as

$$\begin{aligned} l^{(t)}(\boldsymbol{\mu}_1, \dots, \boldsymbol{\mu}_M, \boldsymbol{\Sigma}_1, \dots, \boldsymbol{\Sigma}_M | \mathbf{z}_1, \dots, \mathbf{z}_N) \\ = \sum_{i=1}^N \left[\sum_{j=1}^M \Delta_{i,j}^{(t)} \ln \left(\omega_j^{(t)} g_j \left(\mathbf{z}_i; \boldsymbol{\mu}_j^{(t)}, \boldsymbol{\Sigma}_j^{(t)} \right) \right) \right]. \end{aligned} \quad (5)$$

We evaluate this function only to check for the convergence of the EM algorithm.

Let $\Delta_{i,j}$ symbolize the association of the i th data point to the j th cluster represented by the j th Gaussian distribution. Therefore, we have

$$\Delta_{i,j} = \begin{cases} 1; & \text{if } \mathbf{z}_i \text{ belongs to the cluster } g_j, \\ 0; & \text{otherwise.} \end{cases}$$

It is clear that $P(\Delta_{i,j} = 1) = \omega_j$ and $P(\Delta_{i,j} = 0) = 1 - \omega_j$. However, both $\Delta_{i,j}$ and ω_j are unknown. In the t th iteration of the EM algorithm, we first estimate the so-called responsibility variable of each model j for every observation i defined as

$$\hat{\gamma}_{i,j}^{(t)} = \frac{\hat{\omega}_j^{(t-1)} g_j \left(\mathbf{z}_i; \hat{\mu}_j^{(t-1)}, \hat{\Sigma}_j^{(t-1)} \right)}{\sum_{k=1}^M \hat{\omega}_k^{(t-1)} g_k \left(\mathbf{z}_i; \hat{\mu}_k^{(t-1)}, \hat{\Sigma}_k^{(t-1)} \right)}. \quad (6)$$

We then assign each data point to its corresponding cluster. In particular, for each \mathbf{z}_i , we find $m_i^{(t)} = \arg \max_j \hat{\gamma}_{i,j}^{(t)}$ and set

$$\Delta_{i,j}^{(t)} = \begin{cases} 1; & \text{if } j = m_i^{(t)}, \\ 0; & \text{otherwise.} \end{cases}$$

In the next step of the EM algorithm, we use the calculated responsibilities to update the mean, variance, and weight for each cluster as

$$\hat{\omega}_j^{(t)} = \frac{\sum_{i=1}^N \hat{\gamma}_{i,j}^{(t)}}{\sum_{i=1}^N \sum_{k=1}^M \hat{\gamma}_{i,k}^{(t)}}, \quad (7)$$

$$\hat{\mu}_j^{(t)} = \frac{\sum_{i=1}^N \hat{\gamma}_{i,j}^{(t)} \mathbf{z}_i}{\sum_{i=1}^N \hat{\gamma}_{i,j}^{(t)}}, \quad (8)$$

$$\hat{\Sigma}_j^{(t)} = \frac{\sum_{i=1}^N \hat{\gamma}_{i,j}^{(t)} \left[\mathbf{z}_i - \hat{\mu}_j^{(t)} \right] \left[\mathbf{z}_i - \hat{\mu}_j^{(t)} \right]^T}{\sum_{i=1}^N \hat{\gamma}_{i,j}^{(t)}}. \quad (9)$$

After enough iterations, the values of responsibility, mean, covariance, and weight for each cluster converge as the EM algorithm is guaranteed to converge to a local optimum [36]. The number of iterations required for convergence mainly depends on the convergence criterion. We have observed that the algorithm usually converges in less than ten iterations. In Fig. 2, we visualize the convergence of the mean estimates (cluster centroids) after running eight iterations of the EM algorithm.

When the signals of the users are uniformly drawn from the same QPSK constellation, the weights of the Gaussian distributions are the same, i.e., $\omega_j = \frac{1}{4}$, $j = 1, \dots, 4$. Moreover, using the QPSK modulation and a SIC receiver, at each stage of the SIC, we need to estimate only four Gaussian distributions at each stage. This helps with managing the computational complexity.

The proposed algorithm for joint channel estimation and signal detection is summarized in Algorithm 1. Based on the modulation order m , we fix the weights of each cluster as $\omega_j = \frac{1}{m}$. Next, starting from the first user, we divide the received data into four quadrants and select one point in each cluster as the initial mean and set the initial variance of each cluster to one. Then, we calculate the responsibility and log-likelihood function values using (6) and (5), respectively. Afterwards, we calculate the associated

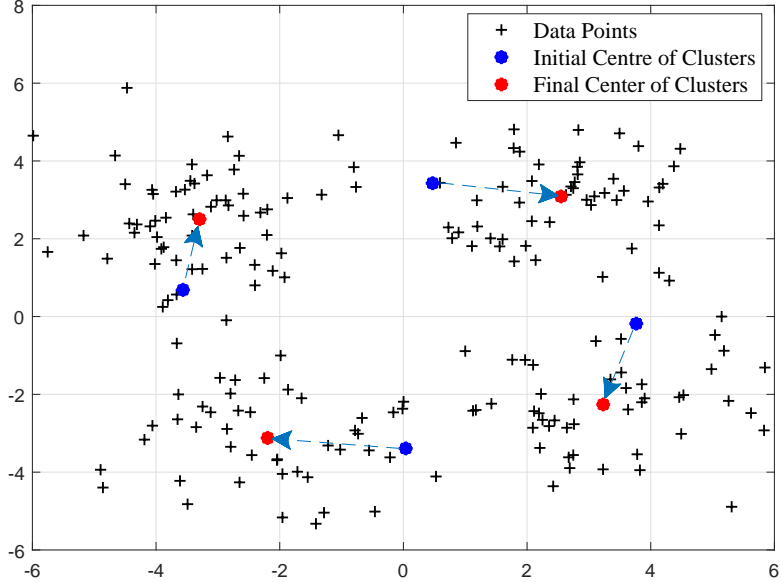


Fig. 2: EM mean convergence after 8 iterations for a single-user scenario, when $\gamma = 7\text{dB}$ and $N = 200$

cluster centroids and covariance matrices (lines 8 to 13 in Algorithm 1). We continue by evaluating the phase of each cluster. Considering that we are using the QPSK modulation, the phase difference between any two adjacent clusters is $\frac{\pi}{2}$. However, due to noise, the phase of each centroid might differ from $\frac{\pi}{4}$, $\frac{3\pi}{4}$, $\frac{5\pi}{4}$, or $\frac{7\pi}{4}$. To minimize the effect of phase rotation, we average the phase difference between the centroid of each cluster and its expected value (Step 15), and update the decision boundaries according to the average phase rotation. Finally, we apply SIC and repeat the algorithm for the next strongest user.

It is important to note that by using SIC, we assume the first four clusters to be Gaussian each consisting of four subclusters, although, the clusters corresponding to the strongest user are not strictly Gaussian in practice. However, roughly speaking, the components of the GMM represent clusters that are of similar shapes. Thus, each cluster is implicitly assumed to follow a Gaussian distribution. For cases where this assumption is overly unrealistic, a natural alternative is to assume that each cluster is also a mixture of normally-distributed subclusters [52].

It is important to note that the GMM clustering algorithm only determines which cluster a data point belongs to. We need an additional step to determine the bit-to-symbol mapping. For this, we use two symbols as a pilot, referred to as demapping pilot, that can be used to estimate the mapping. Determining the mapping with only one symbol is unambiguous when the SNR is not very low. For a robust and accurate performance two symbols per user would be sufficient. We use a minimum mean square error (MMSE) method to estimate the phase rotation due to the channel. The MMSE channel estimate can be

Algorithm 1: GMM-based clustering algorithm for joint channel estimation and signal detection

Input: Received data at BS, number of Gaussian distributions M , modulation order m , and convergence threshold ϵ

Output: Clustered data, mean (centroid) of each cluster $\hat{\mu}$, and covariance of each cluster $\hat{\Sigma}$.

```

1 Set  $\omega_j = \frac{1}{m}$ 
2 for user 1 to  $K$  do
3   Initialize  $\hat{\mu}^{(0)}$  and  $\hat{\Sigma}^{(0)}$  by dividing the received signals on the reference coordinate system
      into  $M$  equal sections and select one point in each section as the initial mean and set the
      initial covariance to one
4   Calculate  $\hat{\gamma}_{i,j}^{(0)}$  according to (6)
5   Calculate log-likelihood function according to (5)
6   Set  $t = 1$ 
7   while  $l^{(t)} - l^{(t-1)} \geq \epsilon$  do
8     Update  $\hat{\mu}^{(t)}$  and  $\hat{\Sigma}^{(t)}$  using (8) and (9)
9     Update  $\hat{\gamma}_{i,j}^{(t)}$  according to (6)
10    Update log-likelihood function according to (5)
11  end
12  Return optimal  $\hat{\mu}$  and  $\hat{\Sigma}$ 
13  Calculate the phase of each cluster centroid ( $\phi_i$ )
14  Calculate the mean phase rotation as  $\phi = \frac{\sum_{i=1}^M \phi_i - M\pi}{M}$ 
15  Update the decision boundaries based on the overall phase rotation due to noise
16  Use the pilot symbol to map each cluster into the mapping bit
17  Apply SIC
18 end

```

written as

$$\hat{h}_{u, \text{MMSE}} = (x_{u,p}^H x_{u,p} + \sigma_n^2)^{-1} x_{u,p}^H y_{u,p}, \quad (10)$$

where $x_{u,p}$ and $y_{u,p}$ are the transmitted and received pilot symbols, respectively. Given the estimated channel phase rotation, we apply the bit-to-symbol mapping. Using our method, the exact phase rotation due to the channel is not required. As we will show later, this is another advantage of our proposed approach over the conventional channel estimation techniques.

In Fig. 3, we compare the SER performance of the proposed GMM-clustering-based approach with

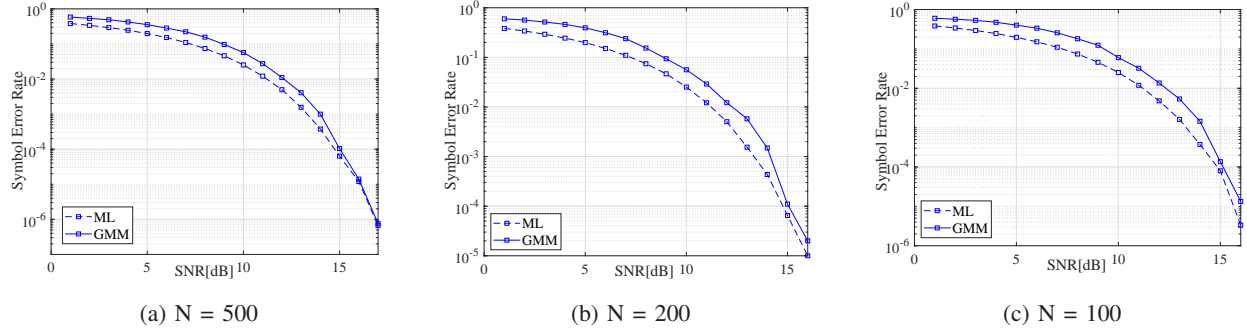


Fig. 3: SER Comparison of the GMM-clustering-based and optimal MLE-based approaches for point-to-point communication.

that of the MLE-based receiver with full CSI knowledge in a single-user scenario with QPSK modulation. As seen in this figure, when the sample size N is large, the GMM-based approach performs close to the optimal MLE-based one with full CSI, and in the high SNR regime, the SERs of the two approaches are almost the same. For small N , there is a small difference in the performance of the two approaches, which can mainly be attributed to the sub-optimal decision boundaries of the GMM due to limited observation.

The performance of the proposed GMM-clustering-based approach for a two-user NOMA communication system is shown in Fig. 4. As seen, the GMM-based approach performs close to the optimal MLE-based approach with full CSI. Similar to the single-user case, as the number of transmitted symbols increase, the SER performance of the GMM-clustering-based approach reaches that of the MLE-based approach with full CSI. The advantage of the clustering-based approach is that each user only needs to send a single pilot (training) symbol for the estimation and elimination of the effect of channel rotation. However, in current systems, to acquire reasonably accurate CSI at the receiver, each user needs to send at least six pilot symbols. This is inefficient when the packet size (number of transmitted symbols) is small [53]. BS does not require a perfect estimation of the channel in our suggested model to eliminate the influence of channel rotation. BS only needs to assign a quadrant to each cluster. We can discover the exact quadrant of each cluster by using a single symbol as a pilot.

IV. ERROR RATE ANALYSIS

In this section, we characterize the error performance of our GMM-based proposed algorithm. In the process of estimating the GMM parameters using EM, there is an estimation error due to the difference between the exact values of the parameters and their estimated values, which we call the EM error. As the EM algorithm is a key step for estimating the GMM parameters, we start by presenting a theorem that gives an upper-bound on the error of the EM algorithm. Then, based on the maximum possible error

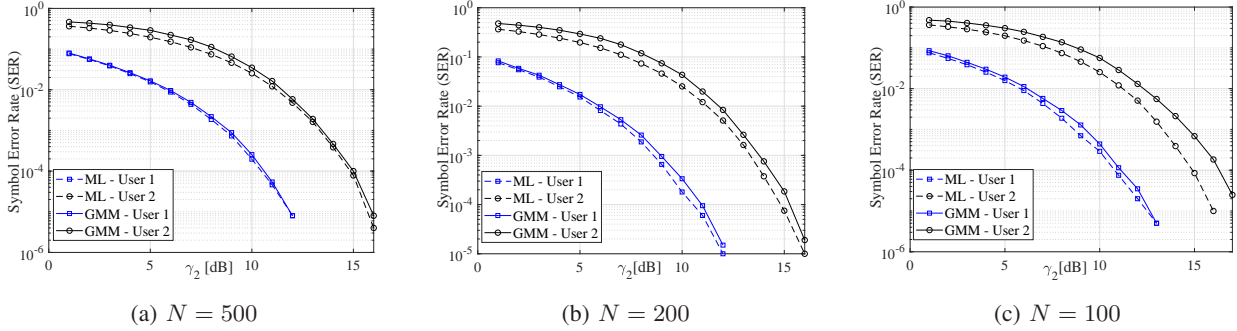


Fig. 4: SER comparison of the GMM-clustering-based and MLE-based approaches for two-user NOMA, when $\gamma_1 - \gamma_2 = 9\text{dB}$.

of the EM algorithm, we find the phase rotation required for updating the boundaries. Finally, using the union bound error probability, we present a mathematical model to evaluate the error rate of our proposed GMM-based joint channel estimation and signal detection algorithm.

Let us consider the distance between the closest cluster centers as R_{\min} and the distance between the farthest cluster centers as R_{\max} . Referring to Fig. 2, we consider the distance between the red dots (final center of the clusters) as R , and we denote the distance between the closest red dots as R_{\min} and the distance between the farthest red dots as R_{\max} . The following theorem characterizes an upper-bound on the EM error.

Theorem 1. *Assume d dimensional received signals and M isotropic Gaussian distributions with weight ω_j , $j \in \{1, \dots, M\}$. Let μ_i^* denote the true mean of cluster i and μ_i^t represent the estimated mean of i -th cluster after t iterations. Suppose $\kappa = \min\{\omega_j\}$, $j \in \{1, \dots, M\}$, $R_{\min} \geq C_0 \min\{d, M\}^{0.5}$ and the initial iterate μ^0 satisfies*

$$\max_{i \in [M]} \|\mu_i^0 - \mu_i^*\|_2 \leq \frac{1}{2} R_{\min} - C_1 \min\{d, M\}^{0.5} \log \left(\max\left\{\frac{M}{\kappa^2}, R_{\max}, \min\{d, M\}\right\} \right)^{0.5} \quad (11)$$

where $C_0, C_1 > 0$ are universal constants. As long as the sample size n is large enough so that

$$\frac{\log(n)}{n} \leq \min \left(\frac{\kappa^2}{144\hat{C}_2 M d}, \frac{\kappa^2 \max_{i \in [M]} \|\mu_i^0 - \mu_i^*\|_2^2}{9\hat{C}_3 R_{\max}^2 M d} \right) \quad (12)$$

where $C_2, C_3 > 0$ are universal constants and

$$\begin{aligned} \hat{C}_2 &= C_2 \log \left(M \left(2R_{\max} + \sqrt{d} \right) \right) \\ \hat{C}_3 &= C_3 \log \left(M \left(3R_{\max}^2 + \sqrt{d} \right) \right), \end{aligned}$$

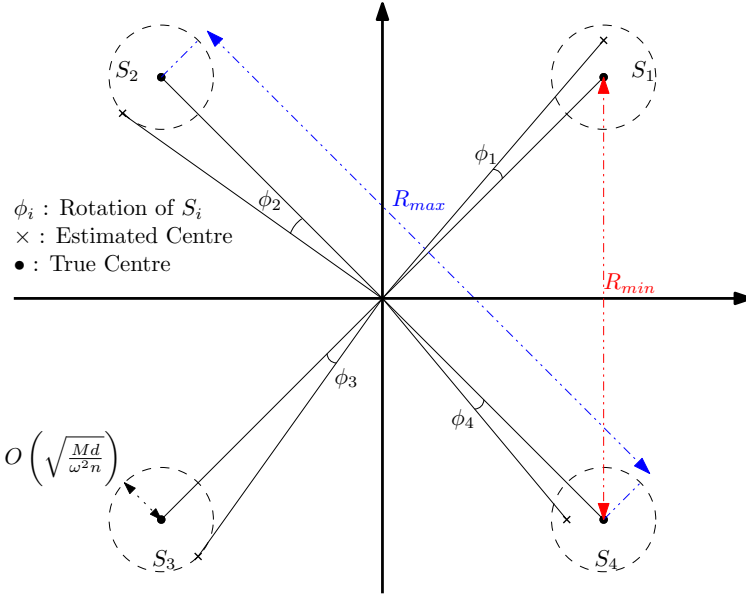


Fig. 5: Illustration of Theorem 1, demonstrating the EM algorithm converges to a point within a ball surrounding the true centre

the subsequent EM iterates $\{\mu_i^t\}_{t=1}^\infty$ satisfy

$$\max_{i \in [M]} \|\mu_i^t - \mu_i^*\|_2 \leq \frac{1}{2^t} \max_{i \in [M]} \|\mu_i^0 - \mu_i^*\|_2 + \frac{3R_{\max}}{\kappa} \left(\frac{\hat{C}_3 M d \log(n)}{n} \right)^{0.5}, \quad (13)$$

with probability at least $1 - \frac{2M}{n}$.

The proof of this theorem is provided in Appendix A. Theorem 1 states that the EM error is bounded. As the iteration number increases, the first term on the right-hand side of (13) converges to zero and the second term dominates. This shows that EM converges to a point within a ball of radius $O\left(\left(\frac{Md}{\omega^2 n}\right)^{0.5}\right)$ of the true centers. Fig. 5 illustrates the essence of Theorem 1. As can be seen, there is a ball of radius $O\left(\left(\frac{Md}{\omega^2 n}\right)^{0.5}\right)$ around each true center and the EM converges to a point within this ball. Averaging the phase difference between each true center and the respective estimated center show the average phase error of the EM algorithm which will be used to update the boundaries of constellation.

Note that the GMM convergence based on Theorem 1 is local since we assumed that the EM algorithm is initialized in the neighborhood of the true centers. To obtain an initial estimate, since we are using the QPSK modulation, we first divide the whole data points into M clusters as defined in Algorithm 1. We then calculate the mean of each cluster. According to our experiments, these centroids are in the neighborhood of the true centers, and therefore can be used for initialization of the EM algorithm. When

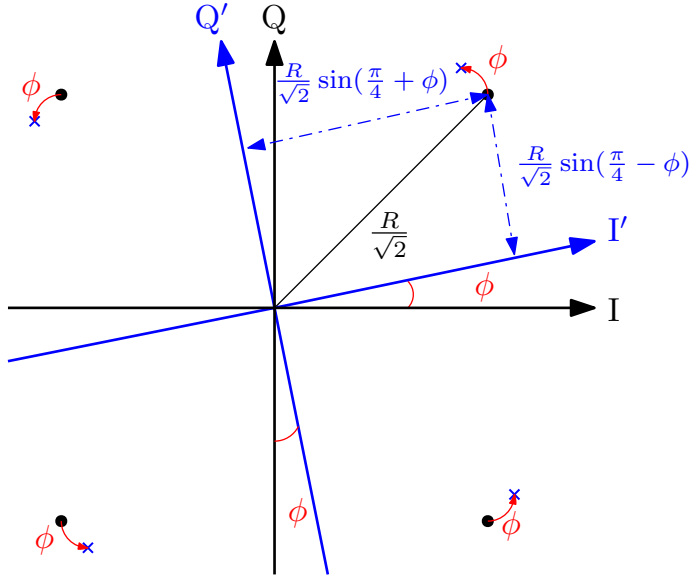


Fig. 6: Constellation rotation due to the EM estimation error.

the BS does not have the knowledge of the modulation scheme, other techniques, e.g., the method of moments [54], can be used for the initialization.

There is an error in the estimation of the mean of each cluster that causes a small rotation of the true values. We average the phase rotations as expressed in Algorithm 1 (line 15). Hence, we consider the whole constellation to be rotated as $\phi = \frac{\sum_{i=1}^M \phi_i - 4\pi}{4}$. Since the constellation has rotated, the decision boundaries for detection should also rotate. Let $P_{correct}$ denote the probability of correct decision for this QPSK constellation based on the rotated constellation (Fig. 6). It can be calculated as follow.

$$P_{correct} = \left(1 - Q \left(\frac{\frac{R}{\sqrt{2}} \sin(\frac{\pi}{4} + \phi)}{\sigma} \right) \right) \times \left(1 - Q \left(\frac{\frac{R}{\sqrt{2}} \sin(\frac{\pi}{4} - \phi)}{\sigma} \right) \right). \quad (14)$$

The aforementioned formula follows from statistical independence of the noise on the quadrature carriers [55]. Accordingly, the SER can be written as

$$P_{SER} = 1 - P_{correct} \approx Q \left(\frac{R \sin(\frac{\pi}{4} + \phi)}{\sqrt{2}\sigma} \right) + Q \left(\frac{R \sin(\frac{\pi}{4} - \phi)}{\sqrt{2}\sigma} \right). \quad (15)$$

To calculate the SER, we calculate the EM error using (13), then we use (15) to calculate the probability of error for our model. Figs. 7 and 8 show the SER values of the QPSK modulation for a SIC receiver based on Algorithm 1. The values are computed according to Theorem 1 and (15). The figures also include the SER values of the optimal MLE-based detector with full CSI.

As described in Theorem 1, with a sufficiently large number of iterations t , the EM estimation error is mainly due to the last term of (13). The value of this term depends on the characteristics of the system,

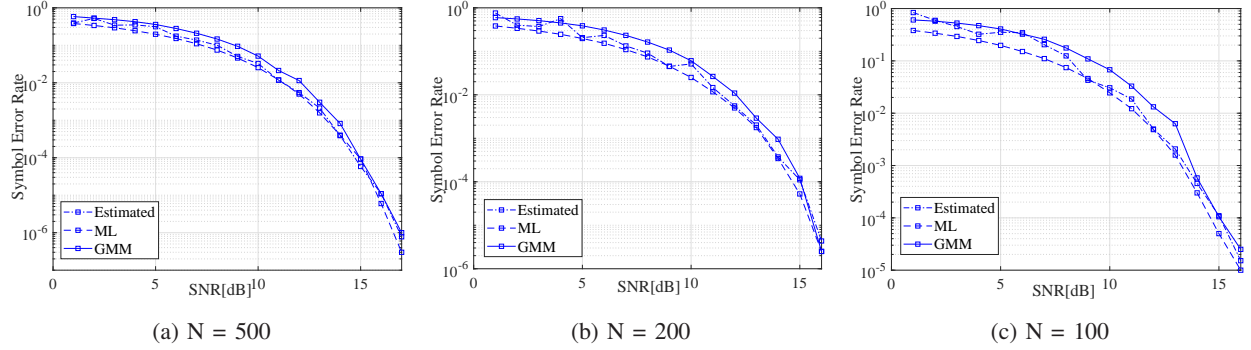


Fig. 7: Comparison of the theoretical SER values for the GMM-clustering-based algorithm as per Theorem 1 with the simulated SER values for both the GMM-clustering-based algorithm and the MLE-based approach with full CSI for point-to-point communication.

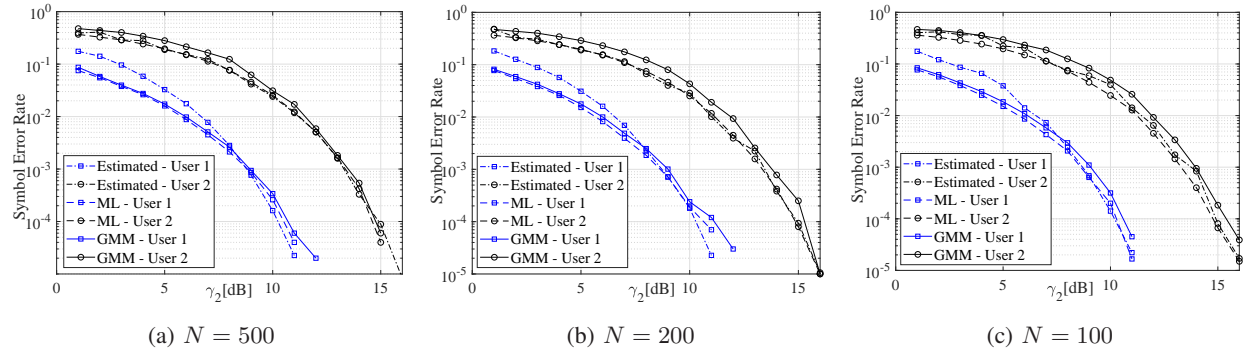


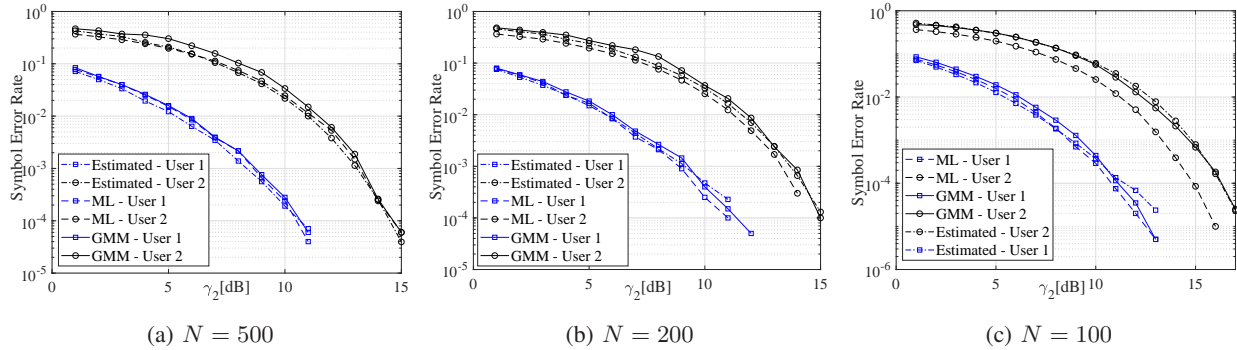
Fig. 8: SER comparison of estimated GMM using Theorem 1, GMM-clustering-based and MLE-based techniques with full CSI for two-user NOMA when $\gamma_1 - \gamma_2 = 9$ dB.

such as dimensions, number of clusters, and modulation order, as well as the constant \hat{C}_3 . Based on the assumptions of the theorem, we can use equation (12) to calculate \hat{C}_3 . However, we need to first compute $\max_{i \in [M]} \|\mu_i^0 - \mu_i^*\|_2^2$, which is the maximum of the distances between the initial estimates of the centroids and their corresponding true values. To calculate this value, we need to run the EM algorithm at least once. By simulating this problem for a few different numbers of symbols, we observed that we can fix the values of \hat{C}_3 for different SNRs and then calculate the SER using (13) and (15). Table I shows the calculated \hat{C}_3 values for different SNRs.

By fixing the value of \hat{C}_3 , we do not go through the process of its calculation. However, it can be different for different numbers of observations. An smart algorithm should be able to adjust this value on its own. The hardship with the value of \hat{C}_3 comes from computing $\max_{i \in [M]} \|\mu_i^0 - \mu_i^*\|_2^2$. This maximum distance is a multiple of σ and can be written as $C'\sigma$ where C' is a universal constant that is the same

TABLE I: Values of \hat{C}_3 for different SNRs and different numbers of symbols.

N	SNR [dB]									
	1	2	3	4	5	6	7	8	9	10
100	0.00131	0.00124	0.00097	0.00075	0.00062	0.00043	0.00031	0.00026	0.00016	0.00010
200	0.00281	0.00187	0.00163	0.00111	0.00071	0.00056	0.00043	0.00033	0.00027	0.00017
500	0.00363	0.00244	0.00183	0.00118	0.00093	0.00078	0.00077	0.00064	0.00057	0.00034

Fig. 9: SER values theoretically predicted by (16) with the simulated ones of the GMM-clustering-based approach and the MLE-based approach with full CSI for a two-user NOMA communication system when $\gamma_1 - \gamma_2 = 9$ dB.

for all SNRs and numbers of observations. Replacing $\max_{i \in [M]} \|\mu_i^0 - \mu_i^*\|_2^2$ with $C'\sigma$, we have

$$\hat{C}_3 \leq \frac{\kappa^2 C' \sigma}{9R_{\max}^2 M d \frac{\log(n)}{n}}, \quad (16)$$

Therefore, we can predict the SER of our GMM-clustering-based algorithm without running the actual GMM algorithm.

In Fig. 9, we compare the simulated SER values for the proposed approach and the MLE-based approach containing full CSI with the theoretically predicted SER values. The values given by (16) predict the SER performance well for both strong and weak users.

V. NUMERICAL RESULTS

To demonstrate that the proposed algorithm performs well as the number of users increases, we consider a scenario where three active users transmit their data to the BS. Fig. 10 shows the SER values for the considered three-user NOMA when the number of symbols is 500 and two symbols have been used for pilot. It can be seen that the proposed algorithm accurately detects the signals.

As we said, in the high SNR regime and when the received powers from the users are sufficiently different, a single pilot symbol is enough for demapping. Given the QPSK modulation and using the

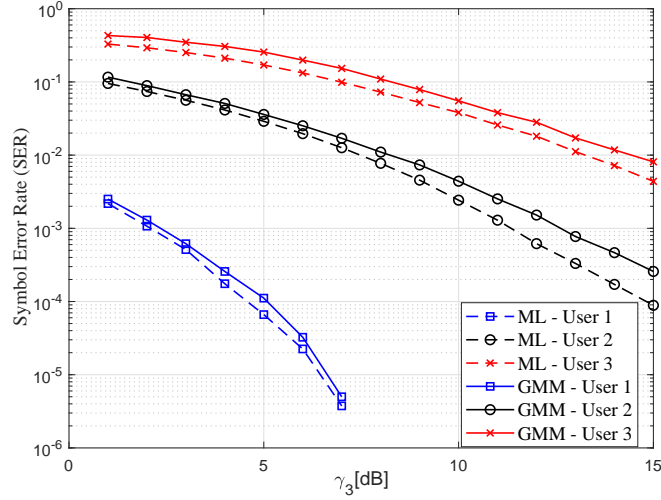


Fig. 10: SER comparison of the GMM-clustering-based and MLE-based techniques with full CSI for three-user NOMA and one symbol pilot when $\gamma_1 - \gamma_2 = 9\text{dB}$ and $N = 500$.

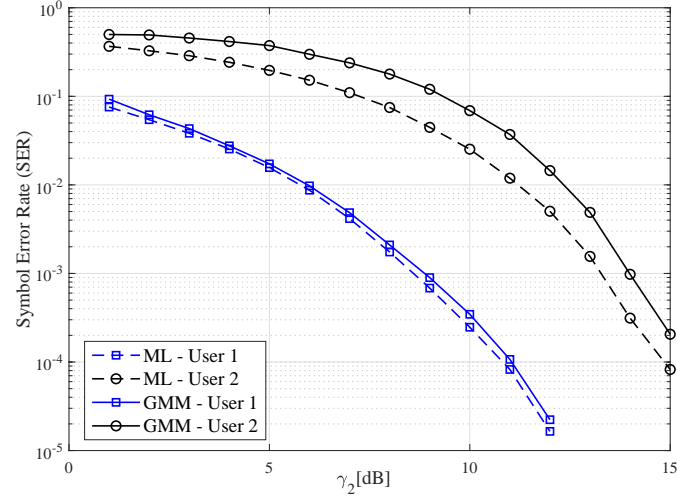


Fig. 11: SER comparison of GMM-clustering-based and MLE-based techniques with full CSI for two-user NOMA and one symbol pilot when $\gamma_1 - \gamma_2 = 9\text{dB}$ and $N = 500$.

one-symbol demapping pilot, we can find the clusters belonging to each quadrant. Then, considering the centroid of each cluster, we can calculate the phase and absolute value of each channel. The performance of one-symbol-based detection is demonstrated in Fig. 11. As can be seen, by using one symbol for demapping, the strong user can approach the performance of MLE-based approach with full CSI. In addition, there is less than one dB gap between the performance of the weak user and the optimal MLE detection.

So far we have compared our proposed joint estimation and detection algorithm with the optimal case of MLE with full CSI. However, in real-world scenarios, obtaining full CSI with only a limited

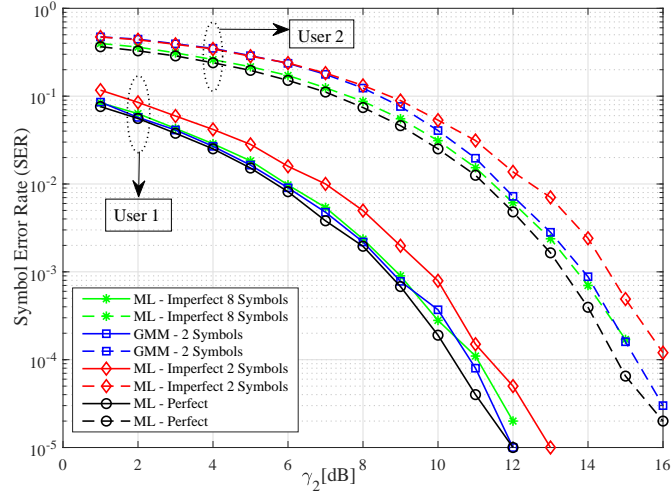


Fig. 12: SER comparison of the proposed GMM-clustering-based approach, MLE-based approach with full CSI, and MLE-based approach with imperfect channel estimation for two-user NOMA when $\gamma_1 - \gamma_2 = 9$ dB and $N = 100$.

number of symbols is not feasible. Fig. 12 shows the performance of our proposed algorithm with two symbols used for demapping in comparison with MLE-based detection with full CSI, MLE-based detection using two symbols for channel estimation, and MLE-based detection using eight symbols for channel estimation. As can be seen, when MLE uses only two symbols for estimating the channel, its performance is significantly inferior to our proposed algorithm using two pilot symbols. For the MLE-based approach to attain a performance close to that of our proposed algorithm, it requires at least eight pilot symbols for channel estimation. For a packet length of 100 symbols, as is shown in Fig. 12, this means our algorithm offers at least six percent improvement in throughput.

Fig. 13 demonstrates the performance of our proposed algorithm in comparison with semi-blind channel estimation. As can be seen, for the same number of pilot symbols, the proposed algorithm offers considerably better performance for all users. For the strongest user, the semi-blind channel estimation approach needs at least ten pilot symbols to perform on a par with the proposed algorithm. This means that the proposed algorithm can result in a throughput that is at least eight percent higher. However, it should be noted that, in such a scenario when the semi-blind approach uses ten pilot symbols, it can lead to better performance in the weak user.

A parameter that should be considered when using the GMM-clustering-based approach is the convergence threshold ϵ . This parameter has a direct impact on the speed of our proposed algorithm as well as its SER performance. As shown in Fig. 14, when the value of ϵ is very small, not only the speed of the algorithm decreases but also the performance degrades due to possible over-estimation. As

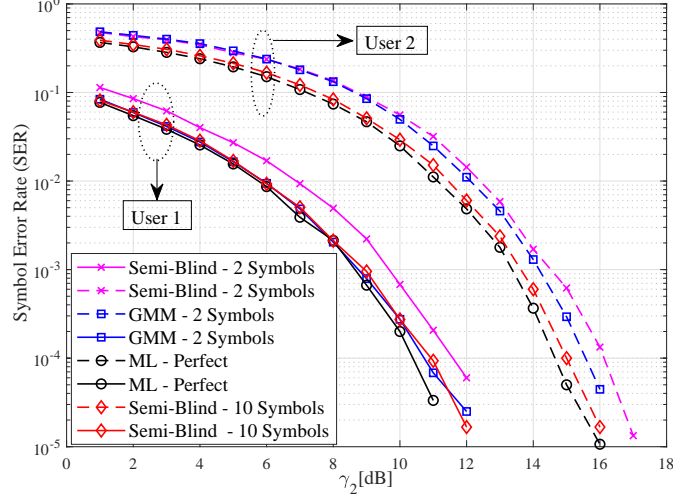


Fig. 13: SER comparison of GMM-clustering-based and Semi-Blind channel estimation for two-user NOMA when $\gamma_1 - \gamma_2 = 9\text{dB}$ and $N = 100$.

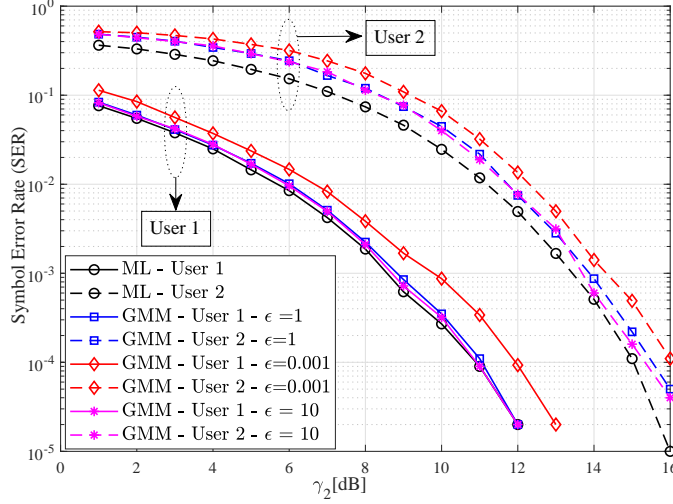


Fig. 14: Impact of ϵ on the SER performance using GMM clustering.

the convergence rate increases, there is an enhancement in SER performance and convergence speed. However, there is an upper limit for convergence rate to avoid underestimation.

When the power difference between two users is small, which means the powers of both users are comparable, the distance between the clusters of the weaker user increases. Hence, there are four close clusters around the center that each belong to a different user. Discriminating these clusters can be hard for the BS as they may be too close to each other or even overlap. Fig. 15 illustrates this point and as can be seen in Fig. 15a, when the power difference between two users is large enough, both users can detect their signals correctly. This is because the distance between clusters are sufficiently large. However, as the power difference between users decreases, see Figs. 15b and 15c, the clusters of weaker users grow

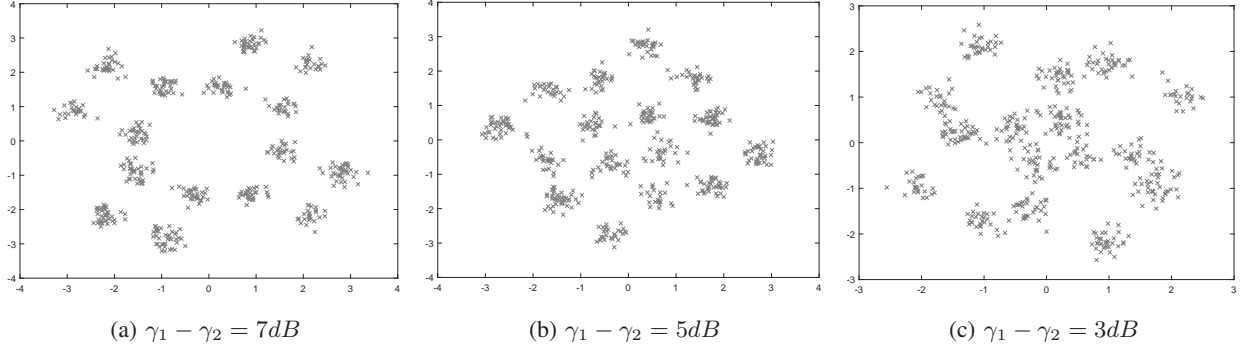


Fig. 15: Constellation of Signals based on their Power Difference for $\gamma_2 = 15dB$

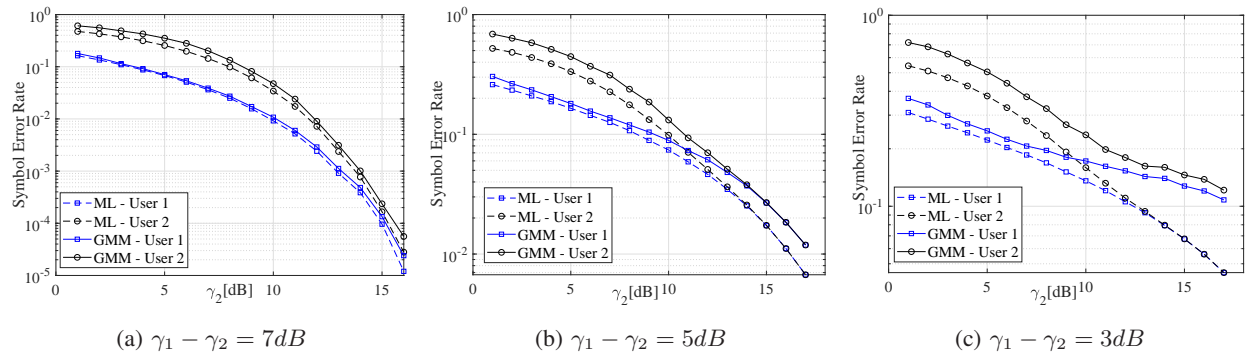


Fig. 16: SER comparison of the GMM-clustering-based and MLE-based techniques for two-user NOMA

farther from each other. Consequently, four clusters appear around the center that belong to different mappings but are rather close to each other.

Fig. 16 demonstrates the SER comparison of a two-user NOMA for three values of power difference between the users. In Fig. 16a, one can see that when the power difference is sufficiently large, the BS can detect the symbols correctly even at low SNR. However, as the power difference decreases, the SER deteriorates for both users. The SER performance of a two-user NOMA when the power difference is lower is shown in Figs. 16b and 16c.

Since GMM comprises expectation and maximization steps, we need to consider the complexity of each step. For a general case, assume we have d dimensions, M clusters, and N samples. In the expectation step, we calculate the determinant and the inverse of the covariance matrix with the complexity order of $\mathcal{O}(MNd^3)$. The maximization step of GMM consists of computing the weight, mean, and covariance for each cluster with the associated complexity of $\mathcal{O}(MN)$, $\mathcal{O}(MN)$, and $\mathcal{O}(MNd)$, respectively. If we achieve convergence after t iterations, the computational complexity of GMM will be in the order of $\mathcal{O}(tMNd^3)$.

VI. A PRACTICAL SCENARIO OF GRANT-FREE TRANSMISSION

So far, we have assumed that the number of users is fixed and the receiver knows this number. This will be used to determine the number of cluster for the GMM algorithm. In this section, we show that our proposed algorithm can be implemented in a real-world scenario where the receiver does not have any prior information except for the modulation scheme used by the transmitters and the power levels.

There are different approaches for discovering the number of clusters such as the elbow method [56], X-means clustering [57], and those based on some information criterion [58]. While the elbow method is subjectively heuristic and X-means clustering is based on a repetitive splitting process, the information-criterion-based approaches determine the number of clusters by maximizing the efficiency that is a measure of fitness. Two main information-criterion-based approaches use the Bayesian information criterion (BIC) [59] and the Akaike information criterion (AIC) [60]. Both of these approaches are based on the penalized-likelihood estimation, i.e., they are MLE methods that penalize the excess free parameters to avoid overfitting.

BIC penalizes the excess free parameters more aggressively compared with AIC. Thus, AIC is known to be prone to overfitting and BIC to underfitting. As the number of observations, N , tends to infinity, the BIC-based approach converges to the true model. However, with a limited number of observations, it is more beneficial to use both AIC and BIC. In other words, when the number of observations is limited, AIC gives an upper bound and BIC a lower bound on the number of clusters. Given the knowledge of the modulation scheme utilized by the users, the BS can detect the number of clusters and subsequently the number of users within the interval between the lower and upper bounds, which is usually small.

We slightly modify the proposed GMM-based clustering algorithm (Algorithm 1) to work even without the knowledge of the number of users. The algorithm is summarized in Algorithm 2. In particular, we first find the average signal power $\mathbb{E}[|\mathbf{y}|^2]$, and if that is larger than the noise power (line 2), we perform the GMM algorithm to cluster the data into m clusters and detect symbols. After applying SIC, we again check the signal power and continue the above process until the signal power falls below the noise power.

We consider a grant-free scenario, where the number of active users is unknown to the BS. Each user randomly selects a power level from a pool of powers $\mathbb{P}_p = \{P_1, P_2, \dots, P_5\}$. We assume each user performs power control such that its average received power at the BS equals the selected power level. The received signal at the BS at time instant i is then given by

$$y_i = \sum_{j=1}^k \sqrt{g_i} h_i x_i + n_i, \quad (17)$$

where $g_i \in \mathbb{P}_p$, h_i is the small-scale fading, and $n_i \sim \mathcal{CN}(0, 1)$, and $\mathbb{E}[|x_i|^2] = 1$. The BS does not have any prior knowledge of k , g_i , and h_i , but it knows \mathbb{P}_p , N_0 , and the modulation used by the users.

Algorithm 2: GMM-based joint channel estimation and signal detection

Input: Received signal \mathbf{y} , noise power N_0 , modulation order m , and convergence threshold ϵ .

Output: Clustered data, mean (centroid) of each cluster $\hat{\mu}$, and covariance of each cluster $\hat{\Sigma}$.

```

1 Set  $\omega_j = \frac{1}{m}$ .
2 while  $P_y > N_0$  do
3   Initialize  $\hat{\mu}^{(0)}$  and  $\hat{\Sigma}^{(0)}$  by dividing the received signals on the reference coordinate system
      into  $m$  equal sections and select one point in each section as the initial mean and set the
      initial covariance to one.
4   Calculate  $\hat{\gamma}_{i,j}^{(0)}$  according to (6).
5   Calculate the log-likelihood function according to (5).
6   Set  $t = 1$ .
7   while  $l^{(t)} - l^{(t-1)} \geq \epsilon$  do
8     Update  $\hat{\mu}^{(t)}$  and  $\hat{\Sigma}^{(t)}$  using (8) and (9).
9     Update  $\hat{\gamma}_{i,j}^{(t)}$  according to (6).
10    Update the log-likelihood function according to (5).
11  end
12  Return optimal  $\hat{\mu}$  and  $\hat{\Sigma}$ .
13  Calculate the phase of each cluster centroid ( $\phi_i$ ).
14  Calculate the mean phase rotation as  $\phi = \frac{\sum_{i=1}^M \phi_i - M\pi}{M}$ .
15  Update the decision boundaries based on the overall phase rotation due to noise.
16  Use the demapping pilot symbols to map each cluster into the mapping bits.
17  Apply SIC and update  $P_y$ .
18 end

```

We first ignore the small-scale fading, i.e., we assume $h_i = 1$ for all users and consider the five power levels in \mathbb{P}_p . The number of users is uniformly distributed between zero and three. At each time-slot, a random number of users start transmitting their information. Fig. 17 shows the performance of Algorithm 2 when we disregard the small-scale fading. We then consider the Rayleigh fading scenario, where $h_i \sim \mathcal{CN}(0, 1)$. Fig. 18 shows the SER of grant-free transmission for a SIC receiver based on Algorithm 2 and its comparison with the MLE with full CSI. As mentioned above, we consider five power levels and each user randomly selects one of the power levels for communication with the BS. At the receiver, we apply Algorithm 2 and average the users' SERs based on their power levels. As can

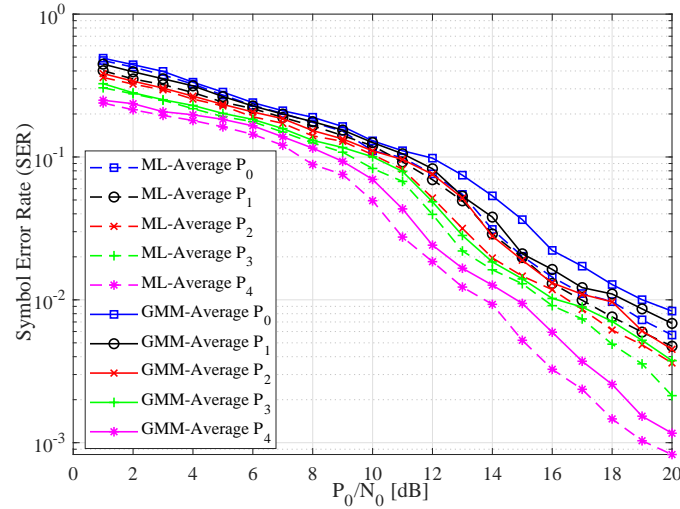


Fig. 17: SER of the GMM-based approach versus the MLE-based one with full CSI for grant-free transmission.

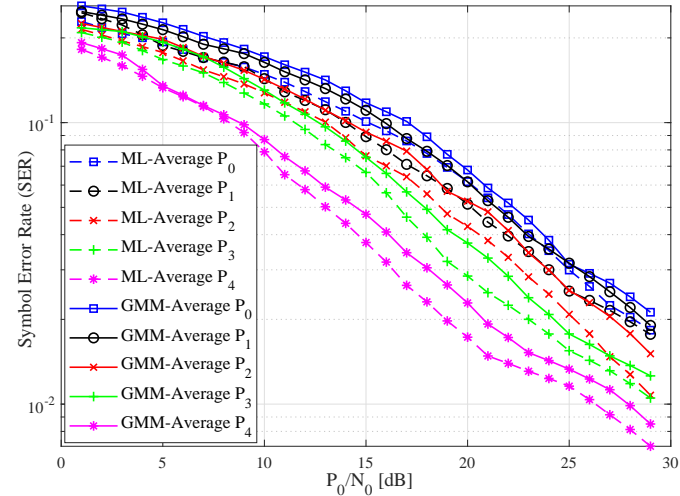


Fig. 18: SER of the GMM-based approach versus the MLE one with full CSI for Grant free transmission with Rayleigh fading.

be seen, the performance of the proposed GMM-based approach with only two pilot symbols is close to that of the MLE with full CSI.

VII. CONCLUSION

In this paper, we proposed employing a semi-supervised machine learning algorithm, i.e., Gaussian mixture model (GMM), to cluster received points at the receiver for joint channel estimation and signal detection in grant-free NOMA. We used a successive interference cancellation scheme to detect data points of each user. We compared the performance of our proposed GMM-clustering-based algorithm with that of the optimal detection method based on maximum likelihood estimation (MLE), which requires full

channel state information (CSI) at the receiver. We showed that using a single pilot symbol for each user, we can reach the performance of the MLE with full CSI. We took one step further and used a single pilot symbol to estimate the channel of all users. The resulting performance was still close to that of the MLE with full CSI. To make a fairer comparison, we also compared the performance of our proposed algorithm with that of the MLE with imperfect channel estimation obtained using a few symbols. We observed that, to attain a similar performance, the MLE needs at least eight symbols when our proposed algorithm uses only two symbols for channel estimation. Furthermore, to reduce the computational burden at the BS, we proposed a theoretical model to calculate the probability of error based on the maximum error of the expectation maximization (EM) algorithm utilized for GMM clustering. Our simulation results showed that the proposed model predicts the probability of error for GMM and MLE well. Our simulations also demonstrated that, when the number of transmitted symbols is moderate or large, the symbol-error-rate performance of the proposed algorithm is on a par with that of the optimal MLE detection. Finally, since the accuracy of the GMM clustering depends on the sample size, we showed that there exists a tradeoff between the accuracy and the block length.

APPENDIX A

PROOF OF THEOREM 1

The proof is based on [41], [42], [61]. Without loss of generality, we focus on the update rule for one of the centers. We start by writing the update rule for the mean as

$$\boldsymbol{\mu}_1^+ - \boldsymbol{\mu}_1^* = \frac{\mathbb{E}[\gamma_1(X, \boldsymbol{\mu})(X - \boldsymbol{\mu}_1^*)]}{\mathbb{E}[\gamma_1(X, \boldsymbol{\mu})]}. \quad (18)$$

Since the vector of the true centers ($\boldsymbol{\mu}^*$) is fixed, we have

$$\mathbb{E}[\gamma_1(X, \boldsymbol{\mu}_1^*)(X - \boldsymbol{\mu}_1^*)] = 0. \quad (19)$$

Hence, we can write

$$\boldsymbol{\mu}_1^+ - \boldsymbol{\mu}_1^* = \frac{\mathbb{E}[(\gamma_1(X, \boldsymbol{\mu}) - \gamma_1(X, \boldsymbol{\mu}^*)) (X - \boldsymbol{\mu}_1^*)]}{\mathbb{E}[\gamma_1(X, \boldsymbol{\mu})]}. \quad (20)$$

We find an upper bound on the norm of the expectation in the numerator. Therefore, we define

$$\boldsymbol{\mu}^t := \boldsymbol{\mu}^* + t(\boldsymbol{\mu} - \boldsymbol{\mu}^*)$$

$$g_X(t) := \gamma_1(X, \boldsymbol{\mu}^t).$$

Subsequently, we have

$$\gamma_1(X, \boldsymbol{\mu}) - \gamma_1(X, \boldsymbol{\mu}^*) = \int_0^1 g'_X(t) dt = \int_0^1 \nabla_{\boldsymbol{\mu}} \gamma_1(X, \boldsymbol{\mu}_1^t)^T (\boldsymbol{\mu}_1^t - \boldsymbol{\mu}_1^*) dt. \quad (21)$$

Computing the integration and applying the expectation, the upper bound can be written as

$$\|\mathbb{E}[(\gamma_1(X, \boldsymbol{\mu}) - \gamma_1(X, \boldsymbol{\mu}^*)) (X - \boldsymbol{\mu}_1^*)]\|_2 \leq V_1 \|\boldsymbol{\mu}_1 - \boldsymbol{\mu}_1^*\|_2 + \sum_{i \neq 1} V_i \|\boldsymbol{\mu}_i - \boldsymbol{\mu}_i^*\|_2 \quad (22)$$

$$\leq M \left(\max_i V_i \right) \left(\max_i \|\boldsymbol{\mu}_i - \boldsymbol{\mu}_i^*\|_2 \right) \quad (23)$$

where

$$V_1 = \sup_{t \in [0,1]} \|\mathbb{E}[\gamma_1(X; \boldsymbol{\mu}^t)(1 - \gamma_1(X; \boldsymbol{\mu}^t))(X - \boldsymbol{\mu}_1^*)(X - \boldsymbol{\mu}_1^t)^T]\|_{op} \quad (24)$$

$$V_i = \sup_{t \in [0,1]} \|\mathbb{E}[\gamma_1(X; \boldsymbol{\mu}^t)\gamma_i(X; \boldsymbol{\mu}^t)(X - \boldsymbol{\mu}_1^*)(X - \boldsymbol{\mu}_i^t)^T]\|_{op}. \quad (25)$$

Considering Z as the label of X , one can write

$$\mathbb{E}[\gamma_1(X; \boldsymbol{\mu}^*)] = \mathbb{E}[\mathbb{P}_{\boldsymbol{\mu}^*}(Z = 1 | X)] = \omega_1 > \kappa. \quad (26)$$

When $\boldsymbol{\mu}$ is in the vicinity of $\boldsymbol{\mu}^*$, we have $\mathbb{E}[\gamma_1(X; \boldsymbol{\mu})] \approx \mathbb{E}[\gamma_1(X; \boldsymbol{\mu}^*)] > \kappa$. According to [41, Lemma 5.2], we know that, as long as $R_{\min} \geq 30 \min\{M, d\}^{0.5}$ and

$$a \geq \frac{1}{2}R_{\min} - \min\{M, d\}^{0.5} \max\{4\sqrt{2}[\log(\frac{R_{\min}}{4})]_+^{0.5}, 8\sqrt{3}, 8\log(\frac{4}{\kappa})\}, \quad (27)$$

for any $\boldsymbol{\mu}_i \in \mathcal{B}(\boldsymbol{\mu}_i^*, a)$ $i \in [M]$, we have $\mathbb{E}[\gamma_i(X; \boldsymbol{\mu})] \geq \frac{3}{4}\kappa$ $i \in [M]$.

Using the above result and the upper bound (19), we have

$$\|\boldsymbol{\mu}_1^+ - \boldsymbol{\mu}_1^*\|_2 = \frac{\|\mathbb{E}[(\gamma_1(X, \boldsymbol{\mu}) - \gamma_1(X, \boldsymbol{\mu}^*)) (X - \boldsymbol{\mu}_1^*)]\|_2}{\mathbb{E}[\gamma_1(X, \boldsymbol{\mu})]} \leq \frac{4M}{3\kappa} \left(\max_i V_i \right) \left(\max_i \|\boldsymbol{\mu}_i - \boldsymbol{\mu}_i^*\|_2 \right). \quad (28)$$

Defining the event $\mathcal{E}_{1,i}$ as

$$\sup_{\boldsymbol{\mu} \in \mathcal{U}} \left\| \frac{1}{n} \sum_{j=1}^n \gamma_i(X_j; \boldsymbol{\mu})(X_j - \boldsymbol{\mu}_i^*) - \mathbb{E}[\gamma_i(X; \boldsymbol{\mu})(X - \boldsymbol{\mu}_i^*)] \right\|_2 \leq 1.5R_{\max} \left(\frac{\hat{C}_3 M d \log n}{n} \right)^{0.5} \quad (29)$$

and the event $\mathcal{E}_{2,i}$ as

$$\sup_{\boldsymbol{\mu} \in \mathcal{U}} \left| \frac{1}{n} \sum_{j=1}^n \gamma_i(X_j; \boldsymbol{\mu}) - \mathbb{E}[\gamma_i(X; \boldsymbol{\mu})] \right| \leq \left(\frac{\hat{C}_2 M d \log n}{n} \right)^{0.5} \quad (30)$$

where $\mathcal{U} = \prod_{i=1}^M \mathcal{B}(\boldsymbol{\mu}^*, R_{\max})$, $\hat{C}_2 = C_2 \log(M(2\sqrt{2}R_{\max} + \sqrt{d}))$, $\hat{C}_3 = C_3 \log(M(6R_{\max}^2 + \sqrt{d}))$, and C_2 and C_3 are universal constants. From [41, Lemmas 5.3 and 5.4], the event $\{\cap_{i \in [M]} \mathcal{E}_{1,i}\} \cap \{\cap_{i \in [M]} \mathcal{E}_{2,i}\}$ for all $i \in [M]$ occurs with the probability at least $1 - \frac{2M}{n}$. Due to the sample size condition (12), we have

$$R_{\max} \left(\frac{\hat{C}_3 M d \log n}{n} \right)^{0.5} \leq \frac{\kappa}{3} \max_{i \in [M]} \|\boldsymbol{\mu}_i^0 - \boldsymbol{\mu}_i^*\|_2 \quad (31)$$

$$\left(\frac{\hat{C}_2 M d \log n}{n} \right)^{0.5} \leq \frac{\kappa}{12}. \quad (32)$$

Using the definition of the event $\mathcal{E}_{2,i}$ for all $i \in [M]$, the second inequality can be written as

$$\sup_{\boldsymbol{\mu} \in \mathcal{U}} \left| \frac{1}{n} \sum_{j=1}^n \gamma_i(X_j; \boldsymbol{\mu}) - \mathbb{E}[\gamma_i(X; \boldsymbol{\mu})] \right| \leq \frac{\kappa}{12}. \quad (33)$$

Considering $\boldsymbol{\mu}^0$ as the initial value of the mean, we can write

$$\|\boldsymbol{\mu}_i^1 - \boldsymbol{\mu}_i^*\|_2 = \frac{\|\frac{1}{n} \sum_{j=1}^n \gamma_i(X_j; \boldsymbol{\mu}^0)(X_j - \boldsymbol{\mu}_i^*)\|_2}{\frac{1}{n} \sum_{j=1}^n \gamma_i(X_j; \boldsymbol{\mu}^0)} \quad (34)$$

$$\leq \frac{\|\mathbb{E}[\gamma_i(X; \boldsymbol{\mu}^0)(X - \boldsymbol{\mu}_i^*)]\|_2 + R_{\max} \left(\frac{\hat{C}_3 M d \log n}{n} \right)^{0.5}}{\mathbb{E}[\gamma_i(X; \boldsymbol{\mu}^0)] - \frac{\kappa}{12}} \quad (35)$$

$$\leq \frac{\|\mathbb{E}[\gamma_i(X; \boldsymbol{\mu}^0)(X - \boldsymbol{\mu}_i^*)]\|_2 + R_{\max} \left(\frac{\hat{C}_3 M d \log(n)}{n} \right)^{0.5}}{\frac{2\kappa}{3}} \quad (36)$$

$$\leq \frac{1}{2} \max_{i \in [M]} \|\boldsymbol{\mu}_i^0 - \boldsymbol{\mu}_i^*\|_2 + \frac{3R_{\max} \left(\hat{C}_3 M d \frac{\log n}{n} \right)^{0.5}}{2\kappa}. \quad (37)$$

Using the above inequality and the first sample size condition, we have

$$\|\boldsymbol{\mu}_i^1 - \boldsymbol{\mu}_i^*\|_2 \leq \frac{1}{2} \max_{i \in [M]} \|\boldsymbol{\mu}_i^0 - \boldsymbol{\mu}_i^*\|_2 + \frac{3R_{\max} \left(\hat{C}_3 M d \frac{\log(n)}{n} \right)^{0.5}}{2\kappa} \quad (38)$$

$$\leq \max_{i \in [M]} \|\boldsymbol{\mu}_i^0 - \boldsymbol{\mu}_i^*\|_2. \quad (39)$$

By applying (34)-(37) over t iterations, we have

$$\max_{i \in [M]} \|\boldsymbol{\mu}_i^t - \boldsymbol{\mu}_i^*\|_2 \leq \frac{1}{2^t} \max_{i \in [M]} \|\boldsymbol{\mu}_i^0 - \boldsymbol{\mu}_i^*\|_2 + \left(1 + \frac{1}{2} + \dots + \frac{1}{2^{t-1}} \right) \frac{3R_{\max} \left(\hat{C}_3 M d \frac{\log(n)}{n} \right)^{0.5}}{2\kappa} \quad (40)$$

$$\leq \frac{1}{2^t} \max_{i \in [M]} \|\boldsymbol{\mu}_i^0 - \boldsymbol{\mu}_i^*\|_2 + \frac{3R_{\max} \left(\hat{C}_3 M d \frac{\log(n)}{n} \right)^{0.5}}{\kappa}. \quad (41)$$

REFERENCES

- [1] ITU, “Minimum requirements related to technical performance for IMT-2020 radio interface (s),” *Report ITU-R*, pp. 2410–2420, 2017.
- [2] M. Framingham, “Growth in connected IoT device,” *International Data Corporation (IDC)*, 2019.
- [3] N. H. Mahmood, S. Böcker, A. Munari, F. Clazzer, I. Moerman, K. Mikhaylov, O. Lopez, O.-S. Park, E. Mercier, H. Bartz *et al.*, “White paper on critical and massive machine type communication towards 6G,” *arXiv preprint*, arXiv:2004.14146, 2020.
- [4] M. B. Shahab, R. Abbas, M. Shirvanimoghaddam, and S. J. Johnson, “Grant-free non-orthogonal multiple access for IoT: A survey,” *IEEE Communications Surveys & Tutorials*, 2020.
- [5] F. Ghanami, G. A. Hodtani, B. Vucetic, and M. Shirvanimoghaddam, “Performance analysis and optimization of NOMA with HARQ for short packet communications in massive IoT,” *IEEE Internet of Things Journal*, vol. 8, no. 6, pp. 4736–4748, 2020.

- [6] M. Aldababsa, M. Toka, S. Gökceli, G. K. Kurt, and O. Kucur, "A tutorial on non-orthogonal multiple access for 5G and beyond," *wireless communications and mobile computing*, vol. 2018, 2018.
- [7] Z. Ma and J. Bao, "Sparse code multiple access (SCMA)," in *Multiple Access Techniques for 5G Wireless Networks and Beyond*. Springer, 2019, pp. 369–416.
- [8] E. Catak, F. Tekce, O. Dizdar, and L. Durak-Ata, "Multi-user shared access in massive machine-type communication systems via superimposed waveforms," *Physical Communication*, vol. 37, p. 100896, 2019.
- [9] Z. Wu, K. Lu, C. Jiang, and X. Shao, "Comprehensive study and comparison on 5G NOMA schemes," *IEEE Access*, vol. 6, pp. 18 511–18 519, 2018.
- [10] M. Vaezi, Z. Ding, and H. V. Poor, *Multiple access techniques for 5G wireless networks and beyond*. Springer, 2019.
- [11] H. Duan, Y. Zhang, and J. Song, "Optimized resource allocation in scalable video broadcasting using LDM and BDM," in *2020 IEEE International Symposium on Broadband Multimedia Systems and Broadcasting (BMSB)*. IEEE, 2020, pp. 1–6.
- [12] X. Dai, Z. Zhang, B. Bai, S. Chen, and S. Sun, "Pattern division multiple access: A new multiple access technology for 5G," *IEEE Wireless Communications*, vol. 25, no. 2, pp. 54–60, 2018.
- [13] L. Dai, B. Wang, Y. Yuan, S. Han, I. Chih-Lin, and Z. Wang, "Non-orthogonal multiple access for 5g: solutions, challenges, opportunities, and future research trends," *IEEE Communications Magazine*, vol. 53, no. 9, pp. 74–81, 2015.
- [14] R. Abbas, T. Huang, B. Shahab, M. Shirvanimoghaddam, Y. Li, and B. Vucetic, "Grant-free non-orthogonal multiple access: A key enabler for 6G-IoT," 2020.
- [15] M. B. Shahab, R. Abbas, M. Shirvanimoghaddam, and S. J. Johnson, "Grant-free Non-orthogonal Multiple Access for IoT: A Survey," *IEEE Communications Surveys & Tutorials*, vol. 22, no. 3, pp. 1805–1838, 2020.
- [16] N. H. Mahmood, H. Alves, O. A. López, M. Shehab, D. P. M. Osorio, and M. Latva-Aho, "Six key features of machine type communication in 6G," in *2020 2nd 6G Wireless Summit (6G SUMMIT)*. IEEE, 2020, pp. 1–5.
- [17] K. B. Letaief, W. Chen, Y. Shi, J. Zhang, and Y.-J. A. Zhang, "The roadmap to 6G: AI empowered wireless networks," *IEEE Communications Magazine*, vol. 57, no. 8, pp. 84–90, 2019.
- [18] T. K. Rodrigues, K. Suto, and N. Kato, "Edge cloud server deployment with transmission power control through machine learning for 6G internet of things," *IEEE Transactions on Emerging Topics in Computing*, 2019.
- [19] J. Kim, H. Ro, and H. Park, "Deep learning-based detector for dual mode ofdm with index modulation," *IEEE Wireless Communications Letters*, 2021.
- [20] F. Tang, Y. Kawamoto, N. Kato, and J. Liu, "Future intelligent and secure vehicular network toward 6G: Machine-learning approaches," *Proceedings of the IEEE*, vol. 108, no. 2, pp. 292–307, 2019.
- [21] M. H. Siddiqui, K. Khurshid, I. Rashid, and A. Ahmed Khan, "Artificial intelligence based 6G intelligent IoT: Unfolding an analytical concept for future hybrid communication systems," *WCSE*, pp. 26–28, 2020.
- [22] W. Zhang, X.-G. Xia, and P.-C. Ching, "Optimal training and pilot pattern design for OFDM systems in Rayleigh fading," *IEEE Transactions on Broadcasting*, vol. 52, no. 4, pp. 505–514, 2006.
- [23] C. Shin, R. W. Heath, and E. J. Powers, "Blind channel estimation for MIMO-OFDM systems," *IEEE Transactions on Vehicular Technology*, vol. 56, no. 2, pp. 670–685, 2007.
- [24] K. Liu, J. P. C. Da Costa, H.-C. So, and A. L. De Almeida, "Semi-blind receivers for joint symbol and channel estimation in space-time-frequency MIMO-OFDM systems," *IEEE Transactions on Signal Processing*, vol. 61, no. 21, pp. 5444–5457, 2013.
- [25] C. R. Murthy, A. K. Jagannatham, and B. D. Rao, "Training-based and semiblind channel estimation for MIMO systems with maximum ratio transmission," *IEEE Transactions on Signal Processing*, vol. 54, no. 7, pp. 2546–2558, 2006.

- [26] S. Jiang, X. Yuan, X. Wang, C. Xu, and W. Yu, "Joint user identification, channel estimation, and signal detection for grant-free noma," *IEEE Transactions on Wireless Communications*, vol. 19, no. 10, pp. 6960–6976, 2020.
- [27] B. Wang, L. Dai, T. Mir, and Z. Wang, "Joint user activity and data detection based on structured compressive sensing for NOMA," *IEEE Communications Letters*, vol. 20, no. 7, pp. 1473–1476, 2016.
- [28] C. Wei, H. Liu, Z. Zhang, J. Dang, and L. Wu, "Approximate message passing-based joint user activity and data detection for NOMA," *IEEE Communications Letters*, vol. 21, no. 3, pp. 640–643, 2016.
- [29] Z. Chen, F. Sohrabi, and W. Yu, "Sparse activity detection for massive connectivity," *IEEE Transactions on Signal Processing*, vol. 66, no. 7, pp. 1890–1904, 2018.
- [30] L. Liu and W. Yu, "Massive connectivity with massive MIMO - part I: Device activity detection and channel estimation," *IEEE Transactions on Signal Processing*, vol. 66, no. 11, pp. 2933–2946, 2018.
- [31] Y. Zhang, Q. Guo, Z. Wang, J. Xi, and N. Wu, "Block sparse Bayesian learning based joint user activity detection and channel estimation for grant-free NOMA systems," *IEEE Transactions on Vehicular Technology*, vol. 67, no. 10, pp. 9631–9640, 2018.
- [32] A. Salari, M. Shirvanimoghaddam, M. B. Shahab, R. Arablouei, and S. Johnson, "Clustering-based joint channel estimation and signal detection for grant-free NOMA," 2020.
- [33] R. J. Rossi, *Mathematical statistics: an introduction to likelihood based inference*. John Wiley & Sons, 2018.
- [34] K. P. Murphy, *Machine learning: a probabilistic perspective*. MIT press, 2012.
- [35] C. M. Bishop, "Pattern recognition and machine learning (information science and statistics)," 2007.
- [36] A. P. Dempster, N. M. Laird, and D. B. Rubin, "Maximum likelihood from incomplete data via the EM algorithm," *Journal of the Royal Statistical Society: Series B (Methodological)*, vol. 39, no. 1, pp. 1–22, 1977.
- [37] T. Hastie, R. Tibshirani, and J. Friedman, *The elements of statistical learning: data mining, inference, and prediction*. Springer Science & Business Media, 2009.
- [38] X.-L. Meng and D. B. Rubin, "Maximum likelihood estimation via the ECM algorithm: A general framework," *Biometrika*, vol. 80, no. 2, pp. 267–278, 1993.
- [39] Z. Zhang, K. L. Chan, Y. Wu, and C. Chen, "Learning a multivariate gaussian mixture model with the reversible jump MCMC algorithm," *Statistics and Computing*, vol. 14, no. 4, pp. 343–355, 2004.
- [40] J. Xu, D. J. Hsu, and A. Maleki, "Global analysis of expectation maximization for mixtures of two gaussians," in *Advances in Neural Information Processing Systems*, 2016, pp. 2676–2684.
- [41] R. Zhao, Y. Li, Y. Sun *et al.*, "Statistical convergence of the em algorithm on gaussian mixture models," *Electronic Journal of Statistics*, vol. 14, no. 1, pp. 632–660, 2020.
- [42] B. Yan, M. Yin, and P. Sarkar, "Convergence of gradient EM on multi-component mixture of gaussians," in *Advances in Neural Information Processing Systems*, 2017, pp. 6956–6966.
- [43] L. Xu and M. I. Jordan, "On convergence properties of the EM algorithm for gaussian mixtures," *Neural computation*, vol. 8, no. 1, pp. 129–151, 1996.
- [44] H. Ashtiani, S. Ben-David, N. Harvey, C. Liaw, A. Mehrabian, and Y. Plan, "Nearly tight sample complexity bounds for learning mixtures of gaussians via sample compression schemes," in *Advances in Neural Information Processing Systems*, 2018, pp. 3412–3421.
- [45] J. Kwon and C. Caramanis, "The EM algorithm gives sample-optimality for learning mixtures of well-separated gaussians," in *Conference on Learning Theory*. PMLR, 2020, pp. 2425–2487.
- [46] K. F. Hasan, C. Wang, Y. Feng, and Y.-C. Tian, "Time synchronization in vehicular ad-hoc networks: A survey on theory and practice," *Vehicular communications*, vol. 14, pp. 39–51, 2018.

- [47] M. Ester, H.-P. Kriegel, J. Sander, X. Xu *et al.*, “A density-based algorithm for discovering clusters in large spatial databases with noise.” in *KDD*, vol. 96, no. 34, 1996, pp. 226–231.
- [48] M. Ankerst, M. M. Breunig, H.-P. Kriegel, and J. Sander, “Optics: ordering points to identify the clustering structure,” *ACM Sigmod record*, vol. 28, no. 2, pp. 49–60, 1999.
- [49] H.-P. Kriegel, P. Kröger, J. Sander, and A. Zimek, “Density-based clustering,” *Wiley Interdisciplinary Reviews: Data Mining and Knowledge Discovery*, vol. 1, no. 3, pp. 231–240, 2011.
- [50] Y. Cheng, “Mean shift, mode seeking, and clustering,” *IEEE transactions on pattern analysis and machine intelligence*, vol. 17, no. 8, pp. 790–799, 1995.
- [51] R. Singh, B. C. Pal, and R. A. Jabr, “Statistical representation of distribution system loads using gaussian mixture model,” *IEEE Transactions on Power Systems*, vol. 25, no. 1, pp. 29–37, 2009.
- [52] T. Hastie and R. Tibshirani, “Discriminant analysis by gaussian mixtures,” *Journal of the Royal Statistical Society: Series B (Methodological)*, vol. 58, no. 1, pp. 155–176, 1996.
- [53] M. Shirvanimoghaddam, M. S. Mohammadi, R. Abbas, A. Minja, C. Yue, B. Matuz, G. Han, Z. Lin, W. Liu, Y. Li, S. Johnson, and B. Vucetic, “Short block-length codes for ultra-reliable low latency communications,” *IEEE Communications Magazine*, vol. 57, no. 2, pp. 130–137, 2019.
- [54] D. Hsu and S. M. Kakade, “Learning mixtures of spherical gaussians: moment methods and spectral decompositions,” in *Proceedings of the 4th conference on Innovations in Theoretical Computer Science*, 2013, pp. 11–20.
- [55] J. G. Proakis, “Digital communications, 1983.”
- [56] P. Bholowalia and A. Kumar, “Ebk-means: A clustering technique based on elbow method and k-means in wsn,” *International Journal of Computer Applications*, vol. 105, no. 9, 2014.
- [57] D. Pelleg, A. W. Moore *et al.*, “X-means: Extending k-means with efficient estimation of the number of clusters.” in *Icml*, vol. 1, 2000, pp. 727–734.
- [58] U. D. Gupta, V. Menon, and U. Babbar, “Detecting the number of clusters during expectation-maximization clustering using information criterion,” in *2010 Second International Conference on Machine Learning and Computing*. IEEE, 2010, pp. 169–173.
- [59] A. A. Neath and J. E. Cavanaugh, “The bayesian information criterion: background, derivation, and applications,” *Wiley Interdisciplinary Reviews: Computational Statistics*, vol. 4, no. 2, pp. 199–203, 2012.
- [60] H. Bozdogan, “Model selection and akaike’s information criterion (aic): The general theory and its analytical extensions,” *Psychometrika*, vol. 52, no. 3, pp. 345–370, 1987.
- [61] R. Vershynin, *High-dimensional probability: An introduction with applications in data science*. Cambridge university press, 2018, vol. 47.